HHS Public Access

Author manuscript

*Neuron*. Author manuscript; available in PMC 2018 April 05.

Published in final edited form as:

*Neuron*. 2017 April 05; 94(1): 207–219.e4. doi:10.1016/j.neuron.2017.03.021.

# Theta Oscillations Rapidly Convey Odor-Specific Content in Human Piriform Cortex

**Heidi Jiang**[1], **Stephan Schuele**[1], **Joshua Rosenow**[2], **Christina Zelano**[1], **Josef Parvizi**[3], **James X. Tao**[4], **Shasha Wu**[4], and **Jay A. Gottfried**[1,5]

[1]Department of Neurology, Northwestern University Feinberg School of Medicine, Chicago, IL 60611, USA

[2]Department of Neurosurgery, Northwestern University Feinberg School of Medicine, Chicago, IL 60611, USA

[3]Department of Neurology & Neurological Sciences, Stanford University, Stanford, CA 94305, USA

[4]Department of Neurology, University of Chicago, Chicago, IL, 60637, USA

[5]Department of Psychology, Northwestern University Weinberg College of Arts and Sciences, Evanston, IL 60208, USA

## Summary

Olfactory oscillations are pervasive throughout vertebrate and invertebrate nervous systems. Such observations have long implied that rhythmic activity patterns play a fundamental role in odor coding. Using intracranial EEG recordings from rare patients with medically resistant epilepsy, we find that theta oscillations are a distinct electrophysiological signature of olfactory processing in the human brain. Across seven patients, odor stimulation enhanced theta power in human piriform cortex, with robust effects at the level of single trials. Importantly, classification analysis revealed that piriform oscillatory activity conveys olfactory-specific information that can be decoded within 110–518 milliseconds of a sniff, and maximally within the theta-frequency band. This temporal window was also associated with increased theta-specific phase coupling between piriform cortex and hippocampus. Together these findings suggest that human piriform cortex has access to olfactory content in the time-frequency domain and can utilize these signals to rapidly differentiate odor stimuli.

Corresponding authors: Heidi Jiang (Lead Contact) (hhjiang@u.northwestern.edu) or Jay A. Gottfried (j-gottfried@northwestern.edu).

The authors declare no financial conflict of interest.

**Author Contributions**

H.J. and J.A.G conceived the study and designed the experiments; H.J., S.S., J.R., C.Z., J.P., J.T., and S.W. performed the experiments; H.J. and J.A.G. analyzed the data, prepared figures, and wrote the manuscript.

Supplemental Information

Tables S1–3, Figures S1–6

## Introduction

Brain oscillations are a ubiquitous hallmark of nervous system function. Coherent rhythmic activity of neuronal assemblies dynamically defines the backdrop of cortical excitability, helping to modulate communication and cooperation among different brain areas. Oscillatory activity patterns, commonly observed in both spike activity and local field potentials (LFPs), have been proposed to facilitate a wide array of computations, including sensory coding, feature binding, temporal summation, coincidence detection, information gating, network synchrony, and gain control (Fries, 2005; Panzeri et al., 2010; Schroeder and Lakatos, 2009). Increasing evidence suggests that oscillations in the human brain are affiliated with cognitive operations related to attention, perception, sensorimotor integration, learning, and memory (Canolty and Knight, 2010; Jacobs and Kahana, 2010; Mukamel and Fried, 2012).

Some of the earliest research demonstrating rhythmic bursts of electrical activity was pioneered in the olfactory system (Adrian, 1942). Adrian showed that the mere act of sniffing entrains oscillatory activity in the hedgehog piriform cortex (PC), priming the olfactory system in advance of odor stimulation. Subsequent work in both vertebrates and invertebrates has established that odor-induced oscillatory activity is a distinctive neural signature throughout much of the olfactory system, including the olfactory bulb, PC, and entorhinal cortex (Bressler and Freeman, 1980; Fontanini and Bower, 2006; Kay and Stopfer, 2006; Laurent et al., 2001). Both slow oscillations in phase with respiration, and faster oscillations in the beta and gamma frequency ranges, have been described. Whether the human olfactory brain engages the same electrophysiological mechanisms as identified in animal models remains poorly understood. Traditional efforts to characterize the neural substrates of human olfaction have taken one of three forms. Lesion studies in patients with damage to the temporal or frontal lobes brought initial insights to the brain regions supporting odor recognition and identification (Jones-Gotman and Zatorre, 1988), but the large and poorly defined extent of these lesions yield only a coarse understanding of functional neuroanatomy. Alternatively, surface encephalography (EEG) recordings offer millisecond temporal resolution, and have been used to record odor-evoked electrical activity (Lorig, 2000; Rombaux et al., 2006). However, olfactory cortical areas are situated deep within basal frontal and medial temporal lobes, which makes it difficult to reliably localize signal sources (Niedermeyer and da Silva, 2005). Finally, while functional magnetic resonance imaging (fMRI) has contributed substantially to our knowledge of olfactory function in the human brain (Gottfried, 2015), this technique has limited temporal resolution (on the level of seconds).

In comparison to the above approaches, intracranial EEG (iEEG) represents a unique opportunity to study odor processing in the human brain with unrivaled temporal and spatial resolution. To date, only a few iEEG studies have been conducted in the human olfactory system, with limited regional coverage. These investigations have mostly targeted the amygdala, and have shown variable effects of odor stimulation on either oscillatory activity or evoked potentials (Hudry et al., 2001; Hudry et al., 2003; Hughes and Andy, 1979; Jung et al., 2006; Narabayashi et al., 1963). No study has explicitly characterized the time-

frequency dynamics of odor processing in the human PC, nor has any study examined electrophysiological coupling between olfactory-related limbic regions in the human brain.

Here we used olfactory iEEG techniques to record piriform electrophysiological activity while patients took part in a cued odor detection task. This experimental design enabled us to test three specific hypotheses. First, we predicted that oscillations driven by odor in the posterior area of piriform cortex (PPC) would selectively emerge within the theta frequency band, given the prominence of theta activity in olfactory bulb and piriform cortex in tasks associated with odor exploration and discrimination in animal models (Fontanini and Bower, 2005; Kay, 2005; Lowry and Kay, 2007; Margrie and Schaefer, 2003). Second, because each patient received four different odors, we were able to test whether odor-specific content could be decoded from PPC oscillatory activity, and if so, how quickly the human PPC can resolve olfactory perceptual features. Finally, insofar as hippocampal theta is widely thought to support sensory exploration, in both spatial and non-spatial environments (Ekstrom et al., 2005; Tesche and Karhu, 2000), we hypothesized that the presence (vs. absence) of odor would drive theta oscillatory coupling between PPC and hippocampus.

## Results

Seven subjects (6 women, age range 19–61; see Star Methods and Table S1) performed an odor detection task while electrophysiological data were recorded from intracranial depth electrodes (Figure 1A, Figure S1). On each trial, subjects were presented with an odor bottle that contained either one of four unique odorants or odorless air, and judged whether an odor was present or absent (Figure 1B). Analysis of the intracranial data focused on the medial-most electrode contact residing within PPC (5/7 subjects), or within anterior amygdala just posterior to PPC (2/7 subjects). Respiratory airflow data were collected alongside iEEG data (see Star Methods). Sniff rate varied between 0.15 and 0.35 Hz across subjects, based on an estimation of the spectral density of the respiratory time series (Welch's method) (Figure 1C).

### Odor stimulation entrains theta oscillatory activity in human piriform cortex

Visual inspection of single-trial LFP data from electrodes in PPC/amygdala revealed a distinct increase in the amplitude of low-frequency oscillations (theta range ~4–5 Hz), beginning at odor onset in each of the 7 subjects (Figure 1D, right). By comparison, trials in which control (odorless) air was delivered did not exhibit noticeable changes in the LFP waveform (Figure 1D, left). Additional individual traces of the piriform LFP, filtered in both the theta and gamma ranges for each subject (Figure S2), further illustrate the prominence of theta activity at the onset of odor stimulation.

Based on these initial observations, we performed a broadband (1–100 Hz) spectral characterization of the time-frequency properties in PPC, enabling us to test whether odor stimulation selectively modulates oscillatory power in the theta frequency range or has a more generalized effect across frequencies. For each subject, the trial-wise instantaneous power was extracted at each frequency band, for each of the 4 odor conditions and the control (odorless air) condition (using the filter-Hilbert method; see Star Methods). It is evident that the single-trial examples are borne out in the full analysis of spectral power: the

control condition elicited minimal perturbation in time or frequency space, whereas each odor condition elicited a prominent increase in low-frequency power consistently within the theta band in the post-sniff period. This effect was observed in every subject (Figure 2A).

Statistical comparison between the odor condition (combining all trials) and the control air condition (Figure 2B) confirmed that when events were time-locked to sniff onset, theta oscillatory power was significantly higher in the presence of odor than in its absence (cluster correction; (Maris and Oostenveld, 2007). The maximum significant $Z$ statistic varied between 4.2 and 10.4 across subjects ($p < 0.05$, corrected for multiple comparisons for each subject), occurring 300–800 ms after sniff onset (mean = 447 ms, SD = 87.3 ms), at a frequency between 3–6 Hz for 6 of 7 subjects (mean frequency = 4.53 Hz, SD = 0.79); for one subject (Subject 3 [S3], third row) the maximal $Z$ statistic occurred at 14 Hz, with a secondary cluster within theta (peak $Z = 5.9$, $p < 0.05$ corrected), centered at 4.2 Hz, 290 ms after sniff onset. Additionally, a secondary cluster peaking at 10.4 Hz (possibly a theta harmonic), could also be observed in Subject 2, 284 ms after sniff onset. Other than these instances, no other frequency band reached cluster-level significance in any subject.

Interestingly, odor stimulation did not elicit consistent gamma activity in PPC, despite the fact that gamma-frequency oscillations are often reported in animal models of olfaction (Adrian, 1942; Bressler and Freeman, 1980; Kay and Freeman, 1998; Kay, 2003; Litaudon et al., 2008; Neville, 2003; Rojas-Líbano and Kay, 2008). One possible explanation for the lack of an effect is technical: the use of standard spectral analysis methods that rely on signal averaging can miss responses at higher frequencies, because trial-wise responses may occur at different phases of the sniff. Therefore, to focus more specifically on the question of odor-induced gamma, we carried out two complementary analyses that offer greater sensitivity in identifying high-frequency activity. In a first analysis, we applied an algorithm to detect the emergence of gamma on a trial-by-trial basis (Coon and Schalk, 2016), minimizing the impact of across-trial jitter that might otherwise obscure identification of stimulus-induced gamma (see Star Methods). After realigning individual trials to above-threshold onset of gamma activity, we found minimal differences between odor and no odor trials across subjects, for both low and high gamma (Figure S3), with significant increases (odor > no odor) appearing only between 136–140 ms after stimulus onset (low gamma only: $Z = 2.36$, $p = 0.018$; Wilcoxon signed-rank test), as well as significant decreases in low gamma at 218 and 264 ms after stimulus onset ($Z = -2.36$, $p = 0.018$). Although there were a few discrete time-points where gamma significantly differed between odor and no odor, the lack of sustained gamma activity beyond a 4-ms duration suggests that the impact of odor stimulation on gamma oscillatory activity was minimal.

In a second analysis, we used a multitaper method to compute an average spectrum from multiple orthogonal samples of data (Mitra and Pesaran, 1999).This approach has the advantage of overcoming across-trial temporal jitter and low signal-to-noise ratios, which are commonly observed in high-frequency time-series and which are directly relevant to the olfactory system, given that gamma-induced responses may arise at different phases of the sniff. Statistical comparison of odor vs. no odor revealed effects that were highly variable across the 7 subjects: increased gamma activity emerged in three subjects (S1, S5, S6) at < 1s post-sniff and in one subject (S3) at ~1.4 s post-sniff, whereas decreased gamma emerged

in one subject (S2) and no change was found in two subjects (S4 and S7) (maximal significant $Z = 5.91$ (S1), −3.77 (S2), 5.77 (S3), 5.29 (S5), and 6.44 (S6); all $p$'s < 0.001) (Figure S4). Considered alongside the trial-wise method (Coon and Schalk, 2016) above, these follow-up analyses suggest that to whatever extent odor (vs. no odor) might modulate gamma power, the temporal inconsistency of these effects, and their unreliability across subjects, provide inconclusive support for a systematic association between odor presence and gamma activity.

### Odor-elicited theta is regionally localized to piriform cortex

Our initial time-frequency finding of odor-elicited theta activity align well with rodent models in which theta activity coincides with periods of active olfactory exploration (Kay, 2005; Margrie and Schaefer, 2003). Therefore, in follow-up analyses, we tested whether odor oscillations could be robustly identified if piriform LFP activity was delimited to the theta frequency band (3–7 Hz). Time-course plots of PPC theta power demonstrate that when trials were aligned to sniff onset, odor stimulation relative to odorless air was associated with a significant increase ($p < 0.05$) in theta activity in individual subjects (4 of 4 odors in three subjects; 3 of 4 odors in two subjects; 2 of 4 odors in two subjects; Figure 3A and Table S2), which reinforces the idea that the entrainment of theta oscillations was not driven by the act of sniffing per se. In each of the 7 subjects, when data are collapsed across the four odors, theta oscillatory power significantly differed between odor and no odor conditions in PPC/amygdala, with $t$ values ranging between 4.86 and 10.72 (significant after correction for multiple comparisons in 5/7 subjects at $p < 0.05$, and before correction in 2/7 subjects at $p < 0.05$) (Figure 3B). Theta power was also significantly enhanced during odor compared to no odor when we performed a non-parametric statistical test across subjects ($Z = -2.37$, $p = 0.018$; Wilcoxon signed-rank test). Finally, across all electrodes, significant odor > no odor theta was identified exclusively at the PPC/amygdala electrode contacts after Bonferroni correction, apart from one subject who also exhibited significant differences in two electrodes within posterior cingulate cortex (Figure S5A).

We next tested whether odor-driven theta oscillations were regionally selective for PPC. For 6/7 subjects, odor-driven theta was significantly higher in PPC than in all other electrodes after correction for multiple comparisons. The only exceptions were in adjacent PPC electrodes lateral to the medial-most piriform contact (S1, S2, S3, S5), ipsilateral amygdala (S3, S4, S5), contralateral PPC (S2, S3, S5), and contralateral amygdala (S2, S3), where theta power in these electrodes did not significantly differ from theta power in PPC (Figure 3C; Figure S5B). Finally, given the distribution of electrode contacts throughout the medial temporal lobe across subjects, we were able to ask whether there were systematic differences in theta activity as a function of electrode position. Overall it is evident that theta power is maximized within PPC, but is also prominent within the amygdala (Figure S5C). Indeed, multiple linear regression techniques revealed that the spatial position of each electrode (mapped onto a two-dimensional standardized space) was able to predict that electrode's mean theta power during odor presence ($F_{1,240} = 30.69$, $r^2 = 0.21$, $p < 0.001$), with significant partial correlations along the medial-lateral ($r = -0.27$, $p < 0.001$) and anterior-posterior ($r = 0.36$, $p < 0.001$) axes suggesting that theta activity was preferentially enhanced at more medial and anterior locations, within PPC.

## Odor-driven theta power is systematically linked to the inspiratory phase of breathing

In a complementary analysis we tested whether odor-driven theta consistently emerged within a discrete period of the respiratory cycle, on a trial-by-trial basis. Single-trial time-course plots from one subject (patient S1) showed that individual odor trials induced a reliable increase in piriform theta power, arising within 200 ms of sniff onset, whereas no change was evident between pre- and post-sniff for control (odorless air) trials (Figure 4A). Interestingly, when the trial-specific time-course of piriform theta power was mapped onto the corresponding time-course of the sniff waveform, it is clear that for the majority of trials (85.6%), the maximum of theta power occurred before the beginning of expiration (Figure 4B, where each sniff trace terminates at the time-point of maximal theta). In contrast, the few trials in which theta power peaked much later during the sniff were typically those in which theta power was relatively low (compare early traces in dark grey-black to late traces in pale-light grey). Importantly, this trial-wise relationship between sniff phase and theta activity was consistent across subjects (Figure 4C): the maximal odor-elicited theta power was distributed between onset and peak inspiratory flow for 6/7 subjects (circular mean ± SD across subjects = −0.49 rad ± 0.24), and immediately following peak inspiratory flow for Subject 4 (rad = 0.06). Across subjects, theta power was maximal between the onset and end of inspiration for the majority of odor-elicited trials (78.4% ± 10.2%; mean ± SD), while this percentage was significantly lower for odorless air trials (55.6% ± 6.4%, Wilcoxon signed-rank test: $Z = 2.366$, $p = 0.018$).

To quantify the relationship between sniff phase and PPC amplitude across different frequencies, we implemented a phase-amplitude coupling (PAC) analysis (Tort et al., 2008) that computes a modulation index (MI) value for each combination of lower-frequency phase and higher-frequency amplitude (see Star Methods). A phase-frequency plot of the difference in mean PPC power for odor vs. no odor, for each sniff phase (between $-\pi$ and $\pi$) and frequency bin (between 1–100 Hz), shows maximal power arising near $0\pi$-phase and 4-Hz frequency (Figure 4D). Results from the PAC analysis, in which MI values have been averaged across subjects at each frequency bin for both odor (blue) and no odor (grey) conditions (means ± S.E.M.), reveal that the coupling between sniff phase and PPC power is significantly elevated for odor > no odor between 2.76–6.51 Hz, overlapping substantially with theta (Wilcoxon signed-rank test, $Z$'s > 2.17, $p$'s < 0.05) (Figure 4E). These data quantitatively confirm that theta power is modulated by sniff phase, and significantly more so during odor presentation as compared to odorless air.

## Odor-specific information content can be read out from piriform oscillatory activity

In demonstrating that theta activity in human PPC is modulated in the presence (but not the absence) of odor, our findings hold two important implications. First, because delivery of odorless air had no influence on piriform theta oscillation, it is unlikely that pre-stimulus cueing, odor anticipation, or the motor act of sniffing contributed to the post-stimulus theta effect. Indeed, odorless air trials were associated with significantly longer sniff duration (mean = 1.45 s) than odor trials (mean = 1.25 s) across subjects (Figure S6) ($Z = -2.197$, $p = 0.028$; Wilcoxon signed-rank test), though there was no significant difference in sniff inspiratory volume ($Z = -1.521$, $p = 0.128$). Second, the identification of odor-specific theta entrainment implies that piriform oscillations may encode stimulus-specific content, though

it remains possible that the mere presence of odor could elicit general arousal or attention that enhances theta activity, irrespective of stimulus differences between odors.

To confirm whether PPC oscillatory power conveys specific, discriminative information across the set of odor stimuli, we used machine-learning approaches to decode individual odor trials using spectro-temporal features from individual electrodes. As each subject received four different odors during the task, we implemented a multi-level (four-way) nonlinear support vector machine (SVM) classifier such that chance = 25% (see Star Methods). The main prediction was that if content-specific representations were embedded in PPC oscillations, then the SVM classifier should significantly differentiate the four odors; alternatively, if PPC oscillatory activity occurred due to a non-specific effect of odor stimulation, then classifier differentiation of the odors would be unsuccessful.

Our initial analysis, unconstrained with regard to electrodes or frequency bands, considered whether odor content could be decoded from broadband spectral power, and if so, whether decoding was selective for PPC. We found that across subjects, classifier decoding accuracy was consistently high within PPC/amygdala (Figure 5A). In 6 of 7 subjects, 4-way odor decoding at PPC/amygdala electrodes was significantly above chance (Figure 5B, red dots) when compared to shuffled condition labels. In four of these subjects, PPC/amygdala exhibited the highest decoding accuracy across all electrodes (mean = 46%, SD = 7.3%, $p < 0.05$), and in two subjects (S4 and S6), PPC/amygdala exhibited the second highest accuracy rate (mean = 36%, SD = 2%, $p < 0.05$). In other limbic and paralimbic brain regions, electrodes with significant decoding accuracy were less commonly observed in left insular cortex and frontal operculum, left orbitofrontal cortex, and right posterior cingulate cortex. For one subject (S7), no channels could classify odors significantly above chance, including PPC (accuracy = 29%, $p = 0.25$), consistent with the modest effects in the time-frequency plots for this same subject.

Given that each subject was only presented with four odor stimuli, it is possible that results of the decoding analysis could have reflected differences in perceived odor intensity or valence. To address this question, we performed a binary SVM decoding analysis of PPC power across time and frequency between each possible pair of the 4 odorants (total of 6 unique pairs) for each subject, following the same decoding methods employed for the multi-level SVM above. In parallel, we acquired post-hoc behavioral ratings of odor intensity and valence for each odor in 5 patients, and used these ratings to derive perceptual intensity differences for each pair of odorants, enabling us to organize the SVM data into two conditions: the three odorant pairs associated with the *highest* pairwise intensity differences, and the three odorant pairs with the *lowest* pairwise intensity differences. Here the hypothesis was that if odor intensity has a significant impact on stimulus decoding in PPC, then odor pairs with greater differences in perceived intensity should be associated with higher decoding accuracy. Across subjects there was no consistent difference in classification accuracy between odor pairs with greater intensity difference (65.9% ± 5.3%) and lower intensity difference (63.2% ± 3.4%) (Wilcoxon signed-rank test; $Z = -0.94$, $p = 0.34$) (see methods and Table S3). Likewise, no significant differences were observed between odor pairs with greater valence difference (63.3% ± 4.7%) and lower valence difference (65.8% ± 3.3%) ($Z = 0.94$, $p = 0.34$). Taken together, while mean accuracy

increased modestly for odorant pairs with greater perceived intensity differences, our findings do not strongly support the idea that the results of the decoding analysis are exclusively based on odor intensity or odor valence.

The time-frequency decoding analyses described above were based on a post-onset time window between 0 and 1s. However, behavioral and neural findings in animal models indicate that odor information can be resolved in less than 200 ms (Abraham et al., 2004; Cury and Uchida, 2010; Uchida and Mainen, 2003, Wesson et al., 2008), and that odor onset latencies can be discriminated as quickly as 10 ms (Shusterman et al., 2011; Smear et al., 2011). Therefore, to establish the minimal time lag in which human piriform LFPs can resolve odor-specific differences, we plotted the temporal evolution of odor decoding. For the PPC/amygdala contacts with the most significant decoding accuracy, we performed multi-way classification at sliding window intervals, which revealed significant classification accuracy beginning 110 ± 58 ms (mean ± SEM) across subjects (mean accuracy = 38%, SD = 3%, $p < 0.05$), and with maximal classification accuracy 518 ± 100 ms after onset (mean accuracy = 45%, SD = 6%, $p < 0.05$) (Figure 5C).

Given that odor stimulation is prominently associated with PPC theta at the single-trial and single-subject levels (cf. Figs. 2–4), we characterized decoding within individual frequency bands in order to assess the contributions of different spectral ranges to odor classification within PPC. This procedure enabled us to evaluate whether classification accuracy was particularly robust in the theta range. Interestingly, we found that decoding accuracy for each and every subject was highest in the theta frequency range (Figure 5D), specifically at center frequencies of 4–6 Hz (4 Hz: mean accuracy ± SD, 38.7% ± 4.8%; $p < 0.05$ in S2–S6; 5 Hz: mean accuracy ± SD, 39.0% ± 5.2%; $p < 0.05$ in S1–S5; 6 Hz: mean accuracy ± SD, 39.2% ± 6.5%; $p < 0.05$ in S1, S2, S4, S5).

## Theta coupling between piriform cortex and hippocampus emerges in presence of odor

While odor-driven theta oscillations in human PPC appear to support rapid differentiation of olfactory stimuli, it is likely that rhythmic activity in other brain regions also plays a role, given the widespread and reciprocal projections between PPC and limbic sites in the medial temporal lobe. There is strong evidence to suggest that the hippocampus is a highly plausible candidate. First, hippocampal extracellular recordings in awake animals have consistently identified theta oscillations during active exploration, information gathering, and sensorimotor integration, including odor exploration and sampling (Lockmann et al., 2016; Macrides et al., 1982; Vanderwolf, 1969). Second, studies have documented synchronous activity between OB/PC and entorhinal cortex/hippocampus during a variety of olfactory tasks including odor detection, learning, and memory (Boeijinga and da Silva, 1989, Chabaud et al., 1999; Kay, 2005; Martin et al., 2007). Therefore, in a final set of analyses (Figure 6), we tested whether active sensing of odor would promote interregional coupling between piriform cortex and hippocampus.

Data from four subjects with contacts in both PPC and anterior hippocampus (AH) were pooled. As a control we additionally examined coupling between PPC and a posterior region in the parahippocampal gyrus (PHG) within these same subjects to ensure that any coupling between PPC and AH was not a general effect (Figure 6A). To demonstrate interregional

oscillatory coupling, we computed the phase-locking value (PLV) across trials, an index of synchrony between electrode pairs, at each frequency band and time point. For the odor condition, we found significant phase locking within a spectro-temporal cluster immediately following stimulus presentation ($p < 0.01$ pixel correction, $p < 0.05$ cluster correction), with the maximum mean $Z$ score occurring 294 ms after sniff onset, at a center frequency of 6.02 Hz within theta (PPC-AH, Figure 6B). For the odorless air condition, only a small punctate cluster in the pre-stimulus period reached significance (peak center frequency at 10.4 Hz, 630 ms pre-sniff). Alternatively, we found no significant phase locking between PPC and PHG in either the odor or odorless air condition (Figure 6C). These findings, unconstrained with regard to frequency space, again underscore the relevance of the theta frequency band as a putative carrier of odor information transfer and exchange.

In a complementary analysis, we specifically examined coupling in the theta range by filtering the LFP data at this frequency (3–7 Hz). To establish whether these effects were specific to olfactory stimulation, we compared PPC-AH theta phase locking in the presence and absence of odor (Figure 6D). For the odor condition, time-course plots of the PLV between PPC and AH revealed peak coupling 300 ms post-odor onset ($p < 0.05$, Bonferroni-corrected), and this effect was significant relative to phase-shuffled data between 1 and 534 ms ($p < 0.05$). Significant coupling was additionally observed for brief periods pre- and post-stimulus ($p < 0.05$). In comparison, for the control (odorless air) condition, while patchy intervals in the pre-and-post stimulation periods were significant ($p < 0.05$), there was no significant phase locking observed within the first 1 s of stimulation of odorless air. Direct comparison of odor and no-odor PLVs showed that phase coupling was significantly enhanced between 200 and 248 ms after sniff onset ($p < 0.05$) (Figure 6D, red vertical bar) during odor presentation, which occurred between the onset and peak of odor decoding within PPC. In contrast, there was no significant phase coupling at any time point between PPC and PHG in either the presence ($p > 0.078$) or absence ($p > 0.21$) of odor, or in comparing odor presence vs. absence ($p > 0.18$) (Figure 6E). Finally, to assess trial-wise consistency of these effects, we plotted circular histograms of the phase differences between PPC and AH, and between PPC and PHG, across all no-odor trials (Figure 6F, top) and all odor trials (Figure 6F, bottom). These data illustrate that PPC-AH odor trials exhibit a nonuniform, narrow PLV distribution centered around 0.39 rad (or 22.2 deg), a profile not observed for any other condition or electrode pair. This result indicates that in the presence of odor, theta-frequency oscillations in PPC and AH become systematically aligned in a majority of trials, and may favor information transmission between these regions.

## Discussion

The prevalence of olfactory oscillations in vertebrate and invertebrate brains has long reinforced the idea that rhythmic activity patterns play a fundamental role in odor coding. Here we show that theta oscillations are a distinct electrophysiological signature of olfactory processing in the human brain. In each of seven subjects, odor stimulation enhanced theta power in human piriform cortex and anterior amygdala, and these effects were robustly observed at the level of single trials. In comparison, no such change in theta power was found in response to odorless control air, ruling out potential confounds related to stimulus anticipation or the motor act of sniffing. Importantly, the use of classification analysis

revealed that piriform oscillatory activity conveys odor-specific content: stimulus decoding of the four odorants emerged within 110 ms (on average) after sniff onset, and was maximal within the theta band. While perceived odor intensity and valence may be partially reflected in our decoding results, these findings suggest that human PPC has ready access to olfactory qualitative information (e.g., garlic, strawberry, almond) in the time-frequency domain and can differentiate odor stimuli within a few hundred milliseconds of a sniff.

The rapid differentiation of odor information in human PPC accords well with a variety of human research findings using other techniques. Psychophysical studies suggest that odor intensity can pre-attentively modulate sniffing behavior as early as 150 ms (Johnson et al., 2003), and human subjects require a sniff of only 420 ms in order to discriminate odors (Laing, 1986). Scalp EEG studies and amygdala iEEG studies report that olfactory-evoked potentials occur in a similar time window of 300–400 ms (Lorig, 2000), and electro-olfactogram (EOG) responses measured at the human epithelium reveal negative potentials arising before 500 ms (Lapid et al., 2011). That odor-specific content can be decoded from piriform theta oscillations beginning at 110 ms and maximally at 518 ms after sniff onset (on average across subjects) highlights a neurophysiological basis for the fast temporal resolution of human olfactory perception.

In contrast, our data suggest that gamma-band activity is not significantly enhanced following odor onset and shows no consistent differential change between odor and no odor trials. Although demonstration of stimulus-induced high-frequency activity can be elusive due to low signal-to-noise ratios and across-trial jitter, we conducted two focused analyses designed to optimize detection of gamma activity, neither of which provided conclusive supporting evidence for a systematic link between gamma and odor presence in human piriform cortex. In light of the fact that olfactory gamma is often observed in animal model systems (Adrian, 1942; Bressler and Freeman, 1980; Kay, 2003; Litaudon et al., 2008; Neville, 2003; Rojas-Líbano and Kay, 2008), it is worth considering why this physiological signature was not identified in our study. Certainly one obvious factor is the difference between species, though gamma effects have been variably reported in human intracranial recordings of the amygdala (Hughes and Andy, 1979; Jung et al., 2006; Narabayashi, 1963). Instead, we speculate that one key difference may be task demands. For example, Beshel and colleagues found that gamma oscillations in the rat olfactory bulb were more robust during fine odor discrimination vs. coarse discrimination, and that gamma increased as olfactory learning progressed (Beshel et al., 2007). By comparison, in our task, humans performed a simple task of sniffing, indicating whether odor was present or absent. This lower-level task simply may not have engaged the sorts of higher-order attentional resources that elicit robust gamma. Interestingly, based on recent data showing that higher rates of breathing (> 4 Hz) enhance odor-evoked gamma power in the rodent olfactory bulb, especially for novel odorants (Rosero and Aylwin, 2011), it is possible that the slow rate of human breathing, and subject familiarity with the odor stimuli, partially accounted for the absence of olfactory gamma in our study. Finally, it is worth noting that simultaneous LFP recordings in olfactory bulb and piriform cortex suggest that odor-related gamma power is much lower and more variable in piriform cortex (Martin et al., 2004; Beshel et al., 2007; Frederick et al., 2016), which may also inform the lack of olfactory gamma in our data-set.

The identification of odor-induced theta in human PPC has interesting physiological implications in context of the non-human animal literature. In rodents, the theta rhythm is often viewed as a respiratory rhythm, given that rats, mice, and hamsters naturally breathe in the theta frequency range (~3–12 Hz). Theta oscillations in synchrony with specific phases of the breathing cycle are most consistently observed in the olfactory bulb (Macrides and Chorover, 1972; Margrie and Schaefer, 2003; Onoda and Mori, 1980), but respiratory coupling to LFP activity and spike firing are also commonly described in PPC (Buonviso et al., 2006; Fontanini and Bower, 2005). As such, there is general consensus that theta oscillations are a manifestation of active stimulus sampling, sensory exploration, and afferent drive, segmented into rhythmic packets of information at the theta frequency of breathing.

Our own data in human PPC bring a slightly different perspective to the above framework. One key point is that humans breathe at a rate of ~0.2 Hz (about once every 5 sec; cf. Figure 1C), a frequency much slower than theta, which in humans is an unsustainable respiratory rate. Nevertheless, we find that odor-induced stimulation is associated with a robust increase in piriform theta oscillations. One plausible interpretation is that the theta frequency is a privileged frequency, conserved throughout the evolution of mammalian brains as an optimal rhythm for mediating information transfer and exchange among “limbic” networks (Seidenbecher et al., 2003). Interestingly, *in vitro* whole-cell recordings in rat piriform cortex (Protopapas and Bower, 2001) suggest that spike trains in individual pyramidal neurons are able to represent low-frequency inputs (< 10 Hz) with greater fidelity than high-frequency inputs (>30 Hz). These observations imply that the theta cycle is a critical functional unit (Wilson et al., 2015) for organizing odor information in PPC, tuned to its intrinsic cellular and synaptic properties (Balu et al., 2004). In context of our findings, it stands to reason that the (evolutionarily) late-arriving human olfactory system continues to exploit the physiological advantages of theta oscillations, even though the human respiratory rate does not drive odor sampling at theta frequency.

What might be the advantages of odor-induced theta activity in human PPC? Empirical and computational studies broadly suggest that theta oscillations are involved in reformatting neural representations within (and across) regions into discrete packets of information (Colgin, 2013; Wilson et al., 2015). Temporal multiplexing of high-frequency oscillations or spike firing at different phases or cycles of theta has been proposed to support various cognitive operations (Colgin, 2013). One intriguing idea is that multiplexed codes are important for stabilizing sensory representations in noisy environments, whereby low-frequency (theta) oscillations can serve as an internal reference frame with which to resolve stimulus ambiguity (Panzeri et al., 2014). The problem of external noise poses a particular challenge for olfactory systems, given that wind speed, wind direction, temperature, and sampling (sniff) behavior, among other factors, can alter the form of an odor stimulus that ultimately makes contact with the sensory receptor sheet. The presence of a theta oscillatory reference frame in human PPC could help overcome imprecisions in spike timing that arise from these sources of odor noise, leading to greater robustness in information coding, as shown in the auditory, visual, and olfactory systems of rats and monkeys (Kayser et al., 2012; Schaefer et al., 2006).

Given that the respiratory cycle itself can serve a reference frame or clock against which to time stimulus events – as convincingly shown in rodent models of olfaction (Shusterman et al., 2011; Wesson et al., 2008) – it is worth considering why an oscillatory reference at theta frequency might be necessary for human olfaction, and why the human respiratory cycle would not suffice. The fact that the human respiratory rate is more than an order of magnitude slower than theta, with individual breaths lasting 1 s or longer, means that the temporal window for stimulus coding would also be in the range of 1 s. A window of this duration may be suboptimal if the relevant information is encoded in a shorter window. To this point, our iEEG data indicate that stimulus representations in PPC can be decoded within a few hundred milliseconds, and rodent studies show that odor information in both olfactory bulb and piriform cortex can be read out from neural responses within one sniff (theta) cycle of ~150 ms (Cury and Uchida, 2010; Miura et al., 2012; Wesson et al., 2008). It thus follows that a theta reference frame in human PPC, partitioning odor-elicited activity into an effective encoding window of 150–200 ms, would define a more relevant temporal scale in which to extract all necessary information about the stimulus.

The potential advantage of an internal reference frame for olfactory processing is also apparent when one considers that not all odor events are time-locked to the onset of sniffing. There are two common instances when this might take place. First, in naturalistic settings, an animal may encounter an odor suddenly, without actively sniffing it out or having predictive knowledge of its occurrence, and without that odor having a reliable latency to the start of inhalation. As suggested for naturalistic sounds in primate auditory cortex (Brasselet et al., 2012), availability of an internal reference frame would provide greater robustness in encoding odor information across different types of stimulus encounters. Second, during mealtime, the “retronasal” olfactory perception of a food placed in the mouth is temporally dissociated from the breathing cycle, typically occurring after swallowing, when odor-laden air is expelled outwards through the nose. This common scenario represents another case where odor-induced theta activity (whether via orthonasal or retronasal route) could provide an appropriate internal clock for organizing olfactory representations with specific information content.

One important proposed function of the theta rhythm is its ability to support long-range network interactions, particularly with regard to modulating the efficacy of signal transmission between brain regions. By estimating phase coupling between piriform cortex and anterior hippocampus, we showed that theta oscillations facilitate the coordination of odor information between these two regions. PPC-AH coupling was limited to the theta-frequency band, appearing selectively during odor presentation, and significantly deviating from the no-odor condition with a mean latency of 224 ms. Notably, the mean theta power in AH did not significantly differ between odor and no-odor conditions (cf. Figure 3C, Figure S5), implying that olfactory stimulation induces a phase resetting of theta activity in hippocampus, bringing its rhythm into tighter temporal alignment with piriform theta. Such temporal dynamics could be critical for enabling exchange of information between these brain areas. Insofar as human fMRI data suggest that odor qualities and categories (e.g., minty, fruity, smoky, etc.) are encoded in PPC (Gottfried et al., 2006; Howard et al., 2009), interregional theta coupling with hippocampus may enable access to stored templates of

previously encountered odors to assist with recollection and identification, perhaps by means of pattern completion (Lengyel et al., 2005).

## STAR Methods

### Contact for Reagent and Resource Sharing

All requests for further information and requests for resources should be directed to and will be fulfilled by the Lead Contact Heidi Jiang (hhjiang@u.northwestern.edu).

### Experimental Model and Subject Details

Electrophysiological data were recorded from nine subjects with intractable epilepsy implanted with depth electrodes targeting PPC and amygdala within the medial temporal lobe (Table S1). Data were acquired at Northwestern Memorial Hospital (six subjects), University of Chicago (two subjects), and Stanford University (one subject), and written informed consent was obtained from all subjects in accordance with the review boards of each institution. Two of nine subjects completed less than ten trials per odor condition of the task, and so we only examined data from the remaining seven subjects in all analyses.

## Method Details

### Data Acquisition

Data were acquired using 128-channel Nihon Kohden recording systems at Northwestern Memorial Hospital and Stanford University Medical Center, and a 256-channel Natus recording system (Natus Medical Incorporated, Pleasanton, CA) at University of Chicago. Signals were sampled between 500–2000 Hz at physician's discretion for each subject and collection site. Depth macro-electrodes were manufactured by Integra (Plainsboro, New Jersey) at Northwestern University and University of Chicago, and by Ad-Tech (Racine, Wisconsin) at Stanford University. These electrodes are cylindrical in shape and have a lead length of 30–40 cm. Each electrode has between 8–12 platinum electrode contacts, and each contact has 2.5 mm of exposed surface. There is a 2.5-mm gap between each contact, resulting in a contact-to-contact electrode spacing of 5 mm. Respiratory airflow data were simultaneously collected using a piezoelectric pressure sensor attached to a nasal cannula at the patient’s nose (Salter Labs). All data were subsequently resampled to 500 Hz offline.

### Electrode Localization

Depth electrodes were localized by first coregistering the pre-operative high-resolution MRI with the post-operative CT using linear affine registration (FLIRT, FSL5) (Smith et al., 2004), and then the electrode coordinates were located in native space (Hermes et al., 2010). Following this, native space MRI and electrode coordinate locations were transformed to Montreal Neurological Institute (MNI) space for across-subject visualization on an average MNI-152 brain (Figure 1A). Across-subject 3D maps overlaid onto the corresponding electrode locations were generated using BrainNet (Xia et al., 2013) (brain rendered using the McConnell Brain Imaging Centre ICBM152).

## Behavioral Paradigm

Each subject was presented with odor bottles containing 1 ml of one of four odorants from a larger set of thirteen odors along with odorless air. Odors included almond, baby powder, banana, cheese, garlic, gasoline, jasmine, orange, peanut butter, pine, rose, sesame, and strawberry. On each trial, subjects were cued to sniff from the odor bottle either verbally or through a computer monitor programmed with PsychToolbox (Brainard, 1997) via MATLAB, and report whether or not they detected an odor. The order of unique odor and odorless air presentation was counterbalanced across trials, and subjects received between 20 and 40 presentations of each odor and odorless air (Table S2).

## Data Preprocessing

All data were analyzed offline in MATLAB using custom scripts in conjunction with functions from the EEGLAB toolbox (Delorme and Makeig, 2004). Data were resampled to 500 Hz, high-pass filtered at 0.1 Hz using a two-way zero phase-lag finite impulse response (FIR) filter, and then notch-filtered at 60 Hz and harmonics to remove line noise. Respiratory data were low-passed at 10 Hz. All channels were visually inspected; noisy and flat channels exceeding 3 standard deviations above or below the mean across channels were rejected, as well as channels with abnormal or interictal spikes. Each channel was referenced to common average (the average signal across electrodes over time). Data were subsequently epoched into trials, which were aligned to the onset of sniff. All trials were manually inspected for artifact; across subjects, an average of 87% of odorless air trials and 89% of odor trials were artifact free and used for subsequent analyses. Percent-retained trials between odor and odorless air conditions was not significantly different ($t_6 = -0.97$, $p = 0.37$).

## Quantification and Statistical Analysis

**Time-frequency power—**Electrophysiological data were filtered between 1 and 100 Hz in 60 steps with center frequencies increasing logarithmically, using a two-way, zero phase lag finite impulse response filter (via eegfilt function from EEGLAB), with 50% overlapping bandwidths. Subsequently, the Hilbert transform was applied to filtered data to extract instantaneous amplitude at each time point and each frequency bin. Trials were aligned to 1s before to 2s after sniff onset, where baseline was defined as 1s before sniff onset. Instantaneous power was *Z*-scored relative to this baseline power across time and all trials for each frequency bin. For each electrode in PPC, we performed statistics on odorless air vs. odor trials for each time point and frequency bin using non-parametric permutation testing. To do this we shuffled odor and air condition labels 1000 times and computed power differences at each pixel each time, thereby building a null distribution of differences between conditions (Maris, 2012). Resulting maps are reported relative to the mean and standard deviation of the null distribution (*Z*-scored). Cluster correction was performed by assessing the maximum cluster size after thresholding pixels at $p < 0.01$ per shuffling iteration, and subsequently applying a $p < 0.05$ cluster size correction using the distribution of collected max clusters (Maris and Oostenveld, 2007), in which only cluster sizes exceeding $p < 0.05$ of the cluster size distribution would be considered significant.

### Theta-restricted analyses

To look more closely into theta power, instantaneous power was extracted between 3–7 Hz, and mean theta power was computed between 0–500 ms after sniff onset for each trial. At the individual subject level we compared mean theta power of odor vs. no odor trials by using a nonparametric bootstrapping technique, resampling 2000 times, and applying a family-wise error Bonferroni correction across electrode number for each subject (alpha of $p = 0.05$).

To examine how theta power varied across discrete electrode locations in the medial temporal lobe, we projected this information onto a standardized anatomical space with reference to the Montreal Neurological Institute (MNI) coordinate system. We defined a 2-dimensional space along the parasagittal axis (x, medial-lateral) and the coronal axis (y, anterior-posterior), onto which the electrodes from all subjects were mapped, with the criterion that only those electrode contacts within the range of $y = +8$ to $-37$, and absolute value of all possible x values were included, to delimit the analysis to medial temporal lobe areas. Note, electrodes were collapsed across the axial plane (z, superior-inferior) between $-40$ and $-5$. We then calculated mean theta power between 0–500 ms after stimulus onset, *Z*-scored across electrodes per subject. For any electrode contacts that fell on the same X/Y coordinate, we calculated the mean power across those contacts. To generate a spatially smoothed 2-D map across x and y axes while minimizing the effects of “empty” X/Y coordinates that did not contain any electrodes, we used a discretized smoothing spline method based on discrete cosine transform (Garcia, 2010). Finally, a standard multiple linear regression was carried out to test the effect of X/Y coordinate location on theta power, and follow-up partial correlations were performed (i.e., correlating X-coordinate information to theta while controlling for the effect of Y-coordinate information on both theta and X, and vice versa).

We next investigated the sniff phase at which theta power was maximal. First we extracted the time point at which theta power was maximal for each trial between sniff onset and 4s afterwards (in order to capture the whole sniff cycle). We then applied the Hilbert transform to the airflow trace and extracted the analytic phase at that time point, whereby a phase of –pi/2 indicates inspiratory onset, 0 indicates inspiratory peak, and pi/2 expiratory onset. Probability density functions of respiratory phase relative to maximal theta across trials were plotted using MATLAB’s ksdensity function, and means of airflow phase were extracted using CircStat within MATLAB (Berens, 2009). Phase-amplitude coupling between airflow phase and filtered signal amplitude at 60 frequencies logarithmically spaced between 1 and 100 Hz was measured by concatenating signals from sniff onset to end of expiration per trial, binning the amplitude of the iEEG signal by sniff phase at 20 windows around the unit circle, and calculating the normalized entropy of the resulting amplitude distribution, i.e., the modulation index (MI) (Tort et al., 2008). This process was performed separately for odor and no odor trials, resampling 1000 times at each frequency bin to match sample sizes across condition. Thus, for each subject, the mean MI was computed at each frequency bin, and submitted across subjects to a nonparametric Wilcoxon signed-rank test.

## Gamma-restricted analyses

We carried out three independent spectral analyses, including the filter-Hilbert method, Morlet wavelets, and multitaper analysis, to determine whether gamma activity could be identified in the presence of odor. For the Hilbert method (and also the wavelet method, which produced very similar results and is therefore not shown), we filtered the ECoG data into low gamma (30–55 Hz) and high gamma (70–150 Hz) frequency bands, and derived the amplitude of the PPC signal using the Hilbert transform. We then adopted a procedure to identify the emergence of high-amplitude transient gamma after stimulus onset, on a trial-by-trial basis (Coon and Schalk, 2016), in order to minimize the effects of across-trial jitter that might otherwise obscure our ability to identify stimulus-induced gamma activity. To this end, for each subject and gamma band (low and high), we applied the detection algorithm as described by Coon and Schalk to generate a unique z-score threshold ($2 \leq Z \leq 6$) across trials that maximized the difference in the absolute number of detections between post-stimulus and pre-stimulus periods. Then we sorted trials according to the timing of the first detection of that threshold crossing, with respect to sniff onset (vertical line at time 0 s), on a subject-by-subject basis. After each trial was re-aligned to the threshold crossing timepoint (such that all trials were aligned to gamma onset), the mean time-series for odor and no odor trials were computed per subject. Significance was assessed per time point across subjects using the Wilcoxon signed-rank test, with a Bonferroni correction of $p < 0.05/2$, for each gamma band investigated. Across all trials, approximately 11% of the trials for each subject did not meet criteria for the $Z$-score threshold and were omitted from the analysis, with an average of 88.6% of odor trials retained and 88.7% of no odor trials retained across subjects.

The multitaper method (Mitra and Pesaran, 1999) involves the use of multiple orthogonal windows (or “tapers”) at different time points, yielding an equal number of orthogonal samples of data. From these data samples, a set of orthogonal estimates of spectral power are obtained, which can be used to compute an average spectrum. By increasing temporal smoothing while reducing spectral variance, multitaper methods have the advantage of overcoming across-trial temporal jitter and low signal-to-noise ratios, which are commonly observed in high-frequency time-series and pose challenges to reliable characterization of gamma activity. We implemented the multitaper analysis using the Chronux toolbox (Mitra and Bokil, 2008; http://chronux.org/), with 5 tapers and a NW product of 3 to examine gamma power at frequencies between 30 and 150 Hz for both odor and air conditions. Resulting power was dB corrected across trials by dividing by the baseline period across trials, per frequency band. Statistical significance was assessed using the cluster correction method as described in the Experimental Procedures section.

## Decoding analysis

We used a statistical learning approach to decode single trials of odor detection using features from individual electrodes. To define features, data from each electrodes were filtered as described above (filter-Hilbert method) and time-frequency power was extracted for 30 logarithmically-spaced frequency bins between 1 and 100 Hz. Filtered data were then epoched between −1s to 1s relative to sniff onset, and the mean of power at each frequency band was extracted for each 10 ms interval to reduce feature dimensionality. Only power from time points after sniff onset were used for classification, as baseline power was used

solely to *Z*-score the features (described below). For each subject a multi-class nonlinear support vector machine classifier using a radial basis function kernel (LIBSVM; Chang and Lin, 2011) was implemented to train between the four odor conditions per electrode. We used leave-one-out cross validation techniques to train on all but one random set of unique odor trials, and then tested on that left-out set of odors. For each training and test iteration, all power between 0–1s was z-scored relative to the baseline of the *training set*, separately for each frequency bin. Because trial sizes differed per condition, we re-computed this procedure 100 times per electrode, resampling *n* trials from each odor, where *n* represents the lowest number of trials across odor conditions. This procedure ensured that the classifier would not be biased by sample size. Decoding accuracy was derived from the mean of this distribution.

Next we used permutation-based nonparametric tests to assess significance of decoding accuracy. To derive a null distribution, we applied the same classification procedure as described above, but used shuffled condition labels to decode shuffled odor labels from a shuffled feature space. This was performed 1000 times per electrode to generate a null distribution of classification accuracies. Significance was assessed per electrode by evaluating the proportion of accuracies from the null distribution that exceed the true distribution.

To investigate the possibility that odor intensity or valence might drive the decoding results, we performed a binary SVM decoding analysis of PPC power across time and frequency (using the same features as described for multi-class SVM) between each possible pair of the 4 odorants (total of 6 unique pairs) for each subject, following the same decoding methods employed for the multi-level SVM above. In parallel, we acquired post-hoc behavioral ratings of odor intensity and valence (rating scale from Lim et al., 2009) for each odor in 5 patients, and used these ratings to derive perceptual intensity differences for each pair of odorants, enabling us to organize the SVM data into two conditions: the three odorant pairs associated with the *highest* pairwise intensity differences, and the three odorant pairs with the *lowest* pairwise intensity differences. By doing so we were able to compare decoding accuracy differences between high and low intensity difference pairs of odors across subjects using a Wilcoxon signed-rank test.

Using one selected PPC/amygdala electrode with highest decoding per subject (for the 6 subjects containing electrodes with significant decoding), we next performed decoding over a sliding window time period between −1s to 2s relative to sniff onset. Every 50 ms, multi-class decoding as outlined above was performed using instantaneous power over 200 ms windows, across the 30 log-spaced frequency bins between 1 and 100 Hz. As described above, because of unequal sample sizes this procedure was performed 100 times per electrode to build a resampling distribution. At each temporal window, significance was assessed against a shuffled null distribution as outlined previously. Finally, using these same electrodes, we then investigated decoding at center frequencies between 1 and 100 Hz with 4 Hz bandwidth, sliding in 1 Hz steps. Features were represented as instantaneous power within the first second of sniff onset; otherwise the classification procedure was identical as described previously.

### Interregional Phase Locking

Frequency-specific coupling between regions was assessed between PPC and anterior hippocampus (AH). To do this we used the cross-regional phase locking value (PLV) (Lachaux et al., 1999), which evaluates the distribution of the phase differences between each pair of electrodes across trials, at each time point; it ranges between 0 (signals are independent; phase distribution is uniform) and 1 (phases are perfectly synchronized). To get an unbiased estimate of PLV, we opted to pool trials from the four subjects who had coverage in both PPC and AH; studies have shown that smaller numbers of observations can lead to a bias in the PLV metric, particularly below 50 samples per condition (Aydore et al., 2013), and no individual subject had more than 40 trials per condition.

For each of these four subjects we selected the piriform electrode on the coronal plane (y-axis) between −2 mm and +4 mm in MNI coordinate space with the highest mean odor-driven theta, and their corresponding anterior hippocampus electrode (between +10 and +14 on the y-axis). In the two subjects with bilateral piriform coverage, we selected the contact with the most significant theta power difference between odor and odorless air conditions, as computed previously. For a control region, we investigated phase locking between those same piriform electrodes and an electrode in parahippocampal gyrus (PHG) (between +28 and +36 on the y-axis).

For each region, data were again filtered between 1–100 Hz in 60 logarithmically increasing center frequencies. Between −1s and 2s relative to sniff onset, the PLV was calculated at each time point for each regional pair (PPC-AH; PPC-PHG) and for each condition. Because there were a greater number of odor present trials compared to odorless trials, we used a resampling procedure to draw 50 trials per condition, 1000 times, to derive a sample estimate of both odor and odorless air PLV at each time point. On each iteration, the PLV was transformed to Rayleigh's Z statistic, and the mean of this distribution was reported. Significance of the PLV per time point was determined using nonparametric testing, whereby the actual mean PLV at each time point was compared against the PLV assessed when the envelope of the AH/PHG signal was shuffled over time (1000 iterations). This generated a null distribution of PLV estimates at each time point with which to compare to the actual PLV, per frequency bin. Correction for multiple comparisons was performed by assessing the maximum cluster size at $p < 0.01$, pixel level per shuffling iteration, with a $p < .05$ cluster correction.

Next we performed the same procedure but focused on data filtered between 3–7 Hz. Significance was determined by the number of instances of PLV from the null distribution (derived again from shuffling the signal envelope) that exceeded the actual PLV at each time point, followed by Bonferroni correction with respect to condition and electrodes at an alpha of $p < 0.05$. Finally, we compared odor and no odor conditions directly at each time point for each regional pair by computing the PLV of each “condition” 1000 times using shuffled condition labels, and comparing the PLV difference across shuffled condition differences against the difference between actual odor and odorless air PLV estimated above. Significance was determined using a Bonferroni correction across electrode (alpha of $p < 0.05$).

To visualize the distribution of phase differences for PPC-AH and PPC-PHG, we calculated the circular mean of phase differences between 0 and 500 ms for each trial. The direction of the vector from the circle center indicates the mean of condition-specific phase distributions (in Figure 6F), and the length of the vector was scaled inversely linearly with its circular variance, such that shorter length indicated greater variance.

### Data and Software Availability

Electrophysiological data were analyzed using MATLAB 2014b, in conjunction with toolboxes including EEGLAB (Delorme and Makeig, 2004), CircStat (Berens, 2009), Chronux (Mitra and Bokil, 2008), and LibSVM (Chang and Lin, 2011). Additionally, FSL (Smith et al., 2004), CTMR (Hermes et al., 2010), and BrainNet (Xia et al., 2013) were used to perform spatial localization and visualization of electrodes.

KEY RESOURCES TABLE

| REAGENT or RESOURCE | SOURCE | IDENTIFIER |
|---|---|---|
| Experimental Models: Organisms/Strains | | |
| Human Epilepsy Patients | Northwestern Memorial Hospital, Stanford Medical Center, University of Chicago Medical Center | N/A |
| Software and Algorithms | | |
| MATLAB | Mathworks | https://www.mathworks.com/ |
| EEGLAB | Delorme and Makeig, 2004 | https://sccn.ucsd.edu/eeglab/ |
| CircStat | Berens, 2009 | http://bethgelab.org/software/circstat/ |
| FSL | Smith et al., 2004 | https://fsl.fmrib.ox.ac.uk/fsl/fslwiki |
| BrainNet | Xia et al., 2013 | https://www.nitrc.org/projects/bnv |
| Chronux | Mitra and Bokil, 2008 | http://chronux.org/ |
| LibSVM | Chang and Lin, 2011 | https://www.csie.ntu.edu.tw/~cjlin/libsvm/ |

## Supplementary Material

Refer to Web version on PubMed Central for supplementary material.

## Acknowledgments

We thank S. Levine, S. Gattas, and V. Rangarajan for help with data acquisition, and T. Kahnt and G. Schalk for valuable discussions. This work was supported by grants to J.A.G from the National Institute on Deafness and Other Communication Disorders (R01DC013243 and R21DC012014) and a training grant to H.J. from the National Science Foundation Graduate Research Fellowship Program Grant (DGE-1324585).

## References

Abraham NM, Spors H, Carleton A, Margrie TW, Kuner T, Schaefer AT. Maintaining accuracy at the expense of speed: stimulus similarity defines odor discrimination time in mice. Neuron. 2004; 44:865–876. [PubMed: 15572116]

Adrian ED. Olfactory reactions in the brain of the hedgehog. J Physiol. 1942; 100:459. [PubMed: 16991539]

Andrews P, Bokil H, Kaur S, Loader C, Maniar H, Mehta S, Mitra P, Nalatore H, Yadav R, Shukla R. The Chronux Manual. 2008

Aydore S, Pantazis D, Leahy RM. A note on the phase locking value and its properties. Neuroimage. 2013; 74:231–244. [PubMed: 23435210]

Balu R, Larimer P, Strowbridge BW. Phasic stimuli evoke precisely timed spikes in intermittently discharging mitral cells. J Neurophysiol. 2004; 92:743–753. [PubMed: 15277594]

Berens P. CircStat: a MATLAB toolbox for circular statistics. J Stat Softw. 2009; 31:1–21.

Beshel J, Kopell N, Kay LM. Olfactory Bulb Gamma Oscillations Are Enhanced with Task Demands. J Neurosci. 2007; 27:8358–8365. [PubMed: 17670982]

Boeijinga PH, da Silva F. Modulations of EEG activity in the entorhinal cortex and forebrain olfactory areas during odour sampling. Brain Res. 1989; 478:257–268. [PubMed: 2924130]

Brainard DH. The psychophysics toolbox. Spatial Vision. 1997; 10:433–436. [PubMed: 9176952]

Brasselet R, Panzeri S, Logothetis NK, Kayser C. Neurons with stereotyped and rapid responses provide a reference frame for relative temporal coding in primate auditory cortex. J Neurosci. 2012; 32:2998–3008. [PubMed: 22378873]

Bressler SL, Freeman WJ. Frequency analysis of olfactory system EEG in cat, rabbit, and rat. Electroencephalogr Clin Neurophysiol. 1980; 50:19–24. [PubMed: 6159187]

Buonviso N, Amat C, Litaudon P. Respiratory modulation of olfactory neurons in the rodent brain. Chem Senses. 2006; 31:145–151. [PubMed: 16339270]

Canolty RT, Knight RT. The functional role of cross-frequency coupling. Trends Cogn Sci (Regul Ed). 2010; 14:506–515. [PubMed: 20932795]

Chabaud P, Ravel N, Wilson DA, Gervais R. Functional coupling in rat central olfactory pathways: a coherence analysis. Neurosci Lett. 1999; 276:17–20. [PubMed: 10586964]

Chang C-C, Lin C-J. LIBSVM. ACM Trans Intell Syst Technol. 2011; 2:1–27.

Colgin LL. Mechanisms and functions of theta rhythms. Annu Rev Neurosci. 2013; 36:295–312. [PubMed: 23724998]

Coon WG, Schalk G. A method to establish the spatiotemporal evolution of task-related cortical activity from electrocorticographic signals in single trials. J Neurosci Methods. 2016; 271:76–85. [PubMed: 27427301]

Cury KM, Uchida N. Robust odor coding via inhalation-coupled transient activity in the mammalian olfactory bulb. Neuron. 2010; 68:570–585. [PubMed: 21040855]

Delorme A, Makeig S. EEGLAB: an open source toolbox for analysis of single-trial EEG dynamics including independent component analysis. J Neurosci Methods. 2004; 134:9–21. [PubMed: 15102499]

Ekstrom AD, Caplan JB, Ho E, Shattuck K, Fried I, Kahana MJ. Human hippocampal theta activity during virtual navigation. Hippocampus. 2005; 15:881–889. [PubMed: 16114040]

Fontanini A, Bower JM. Variable coupling between olfactory system activity and respiration in ketamine/xylazine anesthetized rats. J Neurophysiol. 2005; 93:3573–3581. [PubMed: 15689385]

Fontanini A, Bower JM. Slow-waves in the olfactory system: an olfactory perspective on cortical rhythms. Trends Neurosci. 2006; 29:429–437. [PubMed: 16842864]

Frederick DE, Brown A, Brim E, Mehta N, Vujovic M, Kay LM. Gamma and Beta Oscillations Define a Sequence of Neurocognitive Modes Present in Odor Processing. J Neurosci. 2016; 36:7750–7767. [PubMed: 27445151]

Fries P. A mechanism for cognitive dynamics: neuronal communication through neuronal coherence. Trends Cogn Sci (Regul Ed). 2005; 9:474–480. [PubMed: 16150631]

Garcia D. Robust smoothing of gridded data in one and higher dimensions with missing values. Computational Statistics & Data Analysis. 2010

Gottfried, JA. Handbook of Olfaction and Gustation. Hoboken, NJ: Wiley-Blackwell; 2015. Chapter 13: Structural and Functional Imaging of the Human Olfactory System.

Gottfried JA, Winston JS, Dolan RJ. Dissociable codes of odor quality and odorant structure in human piriform cortex. Neuron. 2006; 49:467–479. [PubMed: 16446149]

Hermes D, Miller KJ, Noordmans HJ, Vansteensel MJ, Ramsey NF. Automated electrocorticographic electrode localization on individually rendered brain surfaces. J Neurosci Methods. 2010; 185:293–298. [PubMed: 19836416]

Howard JD, Plailly J, Grueschow M, Haynes J-D, Gottfried JA. Odor quality coding and categorization in human posterior piriform cortex. Nat Neurosci. 2009; 12:932–938. [PubMed: 19483688]

Hudry J, Ryvlin P, Royet JP, Mauguière F. Odorants elicit evoked potentials in the human amygdala. Cerebral Cortex. 2001; 11:619–627. [PubMed: 11415964]

Hudry J, Perrin F, Ryvlin P, Mauguière F, Royet JP. Olfactory short-term memory and related amygdala recordings in patients with temporal lobe epilepsy. Brain. 2003; 126:1851–1863. [PubMed: 12805107]

Hughes JR, Andy OJ. The human amygdala. I. Electrophysiological responses to odorants. Electroencephalogr Clin Neurophysiol. 1979; 46:428–43. [PubMed: 85539]

Jacobs J, Kahana MJ. Direct brain recordings fuel advances in cognitive electrophysiology. Trends Cogn Sci (Regul Ed). 2010; 14:162–171. [PubMed: 20189441]

Johnson BN, Mainland JD, Sobel N. Rapid olfactory processing implicates subcortical control of an olfactomotor system. J Neurophysiol. 2003; 90:1084–1094. [PubMed: 12711718]

Jones-Gotman M, Zatorre RJ. Olfactory identification deficits in patients with focal cerebral excision. Neuropsychologia. 1988; 26:387–400. [PubMed: 3374800]

Jung J, Hudry J, Ryvlin P, Royet JP, Bertrand O, Lachaux JP. Functional significance of olfactory-induced oscillations in the human amygdala. Cereb Cortex. 2006; 16:1–8. [PubMed: 15829732]

Kay LM, Freeman WJ. Bidirectional processing in the olfactory-limbic axis during olfactory behavior. Behavioral Neuroscience. 1998; 112:541–553. [PubMed: 9676972]

Kay LM. Two species of gamma oscillations in the olfactory bulb: dependence on behavioral state and synaptic interactions. J Integr Neurosci. 2003; 2:31–44. [PubMed: 15011275]

Kay LM. Theta oscillations and sensorimotor performance. Proc Nat Acad Sci. 2005; 102:3863–3868. [PubMed: 15738424]

Kay LM, Stopfer M. Information processing in the olfactory systems of insects and vertebrates. Sem Cell Dev Biol. 2006; 17:433–442.

Kayser C, Ince RAA, Panzeri S. Analysis of Slow (Theta) Oscillations as a Potential Temporal Reference Frame for Information Coding in Sensory Cortices. PLoS Comput Biol. 2012; 8:e1002717. [PubMed: 23071429]

Lachaux JP, Rodriguez E, Martinerie J. Measuring phase synchrony in brain signals. Hum Brain Mapp. 1999; 8:194–208. [PubMed: 10619414]

Laing DG. Identification of single dissimilar odors is achieved by humans with a single sniff. Physiol Behav. 1986; 37:163–170. [PubMed: 3737714]

Lapid H, Shushan S, Plotkin A, Voet H, Roth Y, Hummel T, Schneidman E, Sobel N. Neural activity at the human olfactory epithelium reflects olfactory perception. Nat Neurosci. 2011; 14:1455–1461. [PubMed: 21946326]

Laurent G, Stopfer M, Friedrich RW, Rabinovich MI, Volkovskii A, Abarbanel HD. Odor encoding as an active, dynamical process: experiments, computation, and theory. Annu Rev Neurosci. 2001; 24:263–297. [PubMed: 11283312]

Lengyel M, Huhn Z, Erdi P. Computational theories on the function of theta oscillations. Biol Cybern. 2005; 92:393–408. [PubMed: 15900483]

Lim J, Wood A, Green BG. Derivation and Evaluation of a Labeled Hedonic Scale. Chemical Senses. 2009; 34:739–751. [PubMed: 19833660]

Litaudon P, Garcia S, Buonviso N. Strong coupling between pyramidal cell activity and network oscillations in the olfactory cortex. Neuroscience. 2008; 156:781–787. [PubMed: 18790020]

Lockmann ALV, Laplagne DA, Leão RN, Tort ABL. A respiration-coupled rhythm in the rat hippocampus independent of theta and slow oscillations. J Neurosci. 2016; 36:5338–5352. [PubMed: 27170130]

Lorig TS. The application of electroencephalographic techniques to the study of human olfaction: a review and tutorial. Int J Psychophysiol. 2000; 36:91–104. [PubMed: 10742565]

Lowry CA, Kay LM. Chemical factors determine olfactory system beta oscillations in waking rats. J Neurophysiol. 2007; 98:394–404. [PubMed: 17442770]

Macrides F, Eichenbaum HB, Forbes WB. Temporal relationship between sniffing and the limbic theta rhythm during odor discrimination reversal learning. J Neurosci. 1982; 2:1705–1717. [PubMed: 7143047]

Macrides F, Chorover SL. Olfactory Bulb Units: Activity Correlated with Inhalation Cycles and Odor Quality. Science. 1972; 175:84–87. [PubMed: 5008584]

Margrie TW, Schaefer AT. Theta oscillation coupled spike latencies yield computational vigour in a mammalian sensory system. J Physiol. 2003; 546:363–374. [PubMed: 12527724]

Maris E. Statistical testing in electrophysiological studies. Psychophysiology. 2012; 49:549–65. [PubMed: 22176204]

Maris E, Oostenveld R. Nonparametric statistical testing of EEG- and MEG-data. J Neurosci Methods. 2007; 164:177–190. [PubMed: 17517438]

Martin C, Gervais R, Chabaud P, Messaoudi B, Ravel N. Learning-induced modulation of oscillatory activities in the mammalian olfactory system: the role of the centrifugal fibres. J Physiol-Paris. 2004; 98:467–478. [PubMed: 16274975]

Martin C, Beshel J, Kay LM. An olfacto-hippocampal network is dynamically involved in odor-discrimination learning. J Neurophysiol. 2007; 98:2196–2205. [PubMed: 17699692]

Mitra PP, Pesaran B. Analysis of dynamic brain imaging data. Biophys J. 1999; 76:691–708. [PubMed: 9929474]

Miura K, Mainen ZF, Uchida N. Odor representations in olfactory cortex: distributed rate coding and decorrelated population activity. Neuron. 2012; 74:1087–1098. [PubMed: 22726838]

Mukamel R, Fried I. Human intracranial recordings and cognitive neuroscience. Annu Rev Psychol. 2012; 63:511–537. [PubMed: 21943170]

Narabayashi H, Nagao T, Saito Y, Yoshida M. Stereotaxic amygdalotomy for behavior disorders. Arch Neurol. 1963; 9:1–16. [PubMed: 13937583]

Neville KR, Haberly LB. Beta and gamma oscillations in the olfactory system of the urethane-anesthetized rat. J Neurophysiol. 2003; 90:3921–3930. [PubMed: 12917385]

Niedermeyer, E., da Silva, FHL. Electroencephalography: Basic Principles, Clinical Applications, and Related Fields. Baltimore: Williams & Wilkins; 2005. 1993

Onoda N, Mori K. Depth distribution of temporal firing patterns in olfactory bulb related to air-intake cycles. J Neurophysiol. 1980; 44:29–39. [PubMed: 7420137]

Panzeri S, Brunel N, Logothetis NK, Kayser C. Sensory neural codes using multiplexed temporal scales. Trends Neurosci. 2010; 33:111–120. [PubMed: 20045201]

Panzeri S, Ince RAA, Diamond ME, Kayser C. Reading spike timing without a clock: intrinsic decoding of spike trains. Philos Trans R Soc Lond, B, Biol Sci. 2014; 369:20120467. [PubMed: 24446501]

Protopapas AD, Bower JM. Spike coding in pyramidal cells of the piriform cortex of rat. J Neurophysiol. 2001; 86:1504–1510. [PubMed: 11535694]

Rojas-Líbano D, Kay LM. Olfactory system gamma oscillations: the physiological dissection of a cognitive neural system. Cogn Neurodyn. 2008; 2:179–194. [PubMed: 19003484]

Rombaux P, Mouraux A, Bertrand B, Guerit JM, Hummel T. Assessment of olfactory and trigeminal function using chemosensory event-related potentials. Neurophysiol Clin. 2006; 36:53–62. [PubMed: 16844543]

Rosero MA, Aylwin ML. Sniffing shapes the dynamics of olfactory bulb gamma oscillations in awake behaving rats. European Journal of Neuroscience. 2011; 34:787–799. [PubMed: 21819462]

Schaefer AT, Angelo K, Spors H, Margrie TW. Neuronal oscillations enhance stimulus discrimination by ensuring action potential precision. PLoS Biol. 2006; 4:e163. [PubMed: 16689623]

Schroeder CE, Lakatos P. Low-frequency neuronal oscillations as instruments of sensory selection. Trends Neurosci. 2009; 32:9–18. [PubMed: 19012975]

Seidenbecher T, Laxmi TR, Stork O, Pape HC. Amygdalar and hippocampal theta rhythm synchronization during fear memory retrieval. Science. 2003; 301:846–850. [PubMed: 12907806]

Shusterman R, Smear MC, Koulakov AA, Rinberg D. Precise olfactory responses tile the sniff cycle. Nat Neurosci. 2011; 14:1039–1044. [PubMed: 21765422]

Smear M, Shusterman R, O'Connor R, Bozza T, Rinberg D. Perception of sniff phase in mouse olfaction. Nature. 2011; 479:397–400. [PubMed: 21993623]

Smith SM, Jenkinson M, Woolrich MW, Beckmann CF, Behrens TEJ, Johansen-Berg H, Bannister PR, De Luca M, Drobnjak I, Flitney DE, et al. Advances in functional and structural MR image analysis and implementation as FSL. Neuroimage. 2004; 23:S208–S219. [PubMed: 15501092]

Tesche CD, Karhu J. Theta oscillations index human hippocampal activation during a working memory task. Proc Natl Acad Sci. 2000; 97:919–924. [PubMed: 10639180]

Tort ABL, Kramer MA, Thorn C, Gibson DJ, Kubota Y, Graybiel AM, Kopell NJ. Dynamic cross-frequency couplings of local field potential oscillations in rat striatum and hippocampus during performance of a T-maze task. Proc Natl Acad Sci. 2008; 105:20517–20522. [PubMed: 19074268]

Uchida N, Mainen ZF. Speed and accuracy of olfactory discrimination in the rat. Nat Neurosci. 2003; 6:1224–1229. [PubMed: 14566341]

Vanderwolf CH. Hippocampal electrical activity and voluntary movement in the rat. Electroencephalogr Clin Neurophysiol. 1969; 26:407–418. [PubMed: 4183562]

Wesson DW, Carey RM, Verhagen JV, Wachowiak M. Rapid encoding and perception of novel odors in the rat. PLoS Biol. 2008; 6:e82. [PubMed: 18399719]

Wilson MA, Varela C, Remondes M. Phase organization of network computations. Curr Opin Neurobiol. 2015; 31:250–253. [PubMed: 25679370]

Xia M, Wang J, He Y. BrainNet Viewer: A network visualization tool for Human brain connectomics. PLoS ONE. 2013; 8:e68910. [PubMed: 23861951]

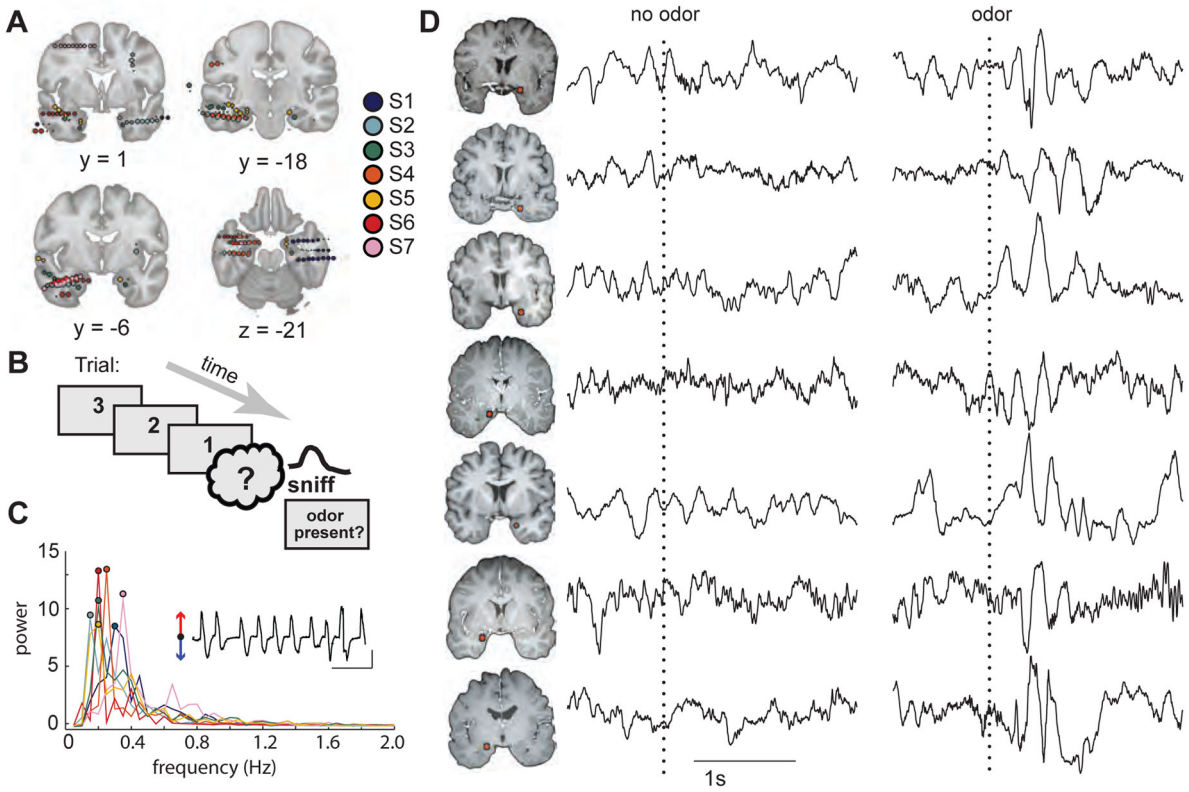


**Figure 1.**

Experimental design and single-trial LFP data in response to odor. (**A**) Electrode locations were coregistered into the Montreal Neurological Institute (MNI) coordinate space and then superimposed on coronal (y-axis) and axial (z-axis) sections of the medial temporal lobe. Electrodes located outside of the brain images indicate extra-cortical contacts. Different colors indicate different subjects. All images are in radiological convention (right side of the image is the left side of the brain). (**B**) During an odor detection paradigm, subjects were cued on each trial to sniff one of four odors or odorless air and to report whether or not they detected an odor. (**C**) Respiratory spectra for each subject are plotted with colors corresponding to those depicted in Fig. 1A. Circles correspond to the peak frequency per subject. Inset, example respiratory trace for subject S1 (red arrow, inspiration; blue arrow, expiration; black horizontal line, 10 s; black vertical line, two *Z*-score units of airflow). (**D**) Single-trial examples of the raw (unfiltered) LFP data from PPC in each subject reveal an increase in theta-frequency oscillatory amplitudes in response to the odor stimulus but not to the control (no odor) stimulus. Trials are aligned to sniff onset (dotted line). Each row represents a different subject (S1 to S7 from top to bottom). Locations of piriform contacts for each subject on separate rows (radiological view). See also Figure S1, S2, and S6.

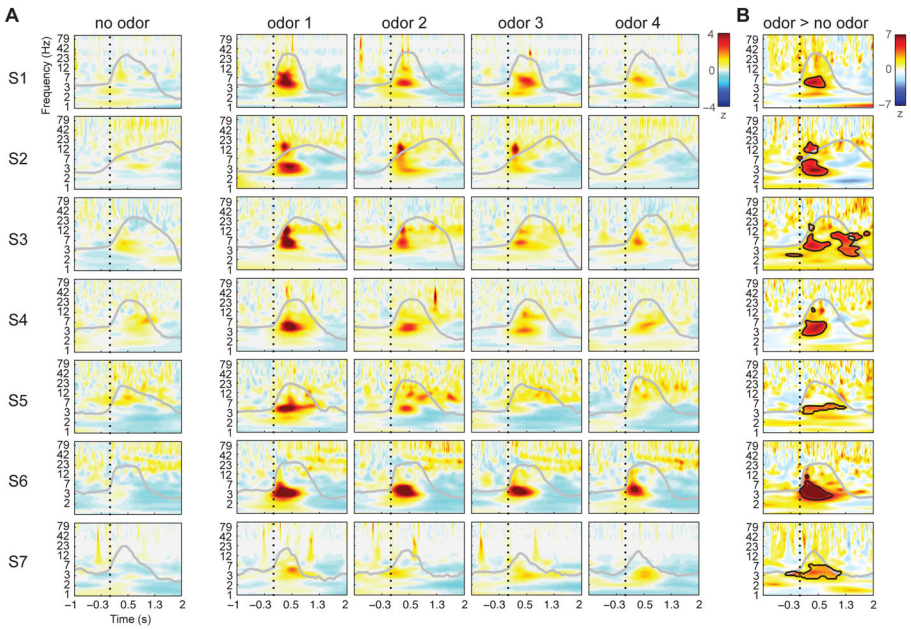


**Figure 2.**

Odor-induced increases in piriform spectral power are selective for the theta-frequency band. (**A**) Time-frequency spectrograms in each subject indicate minimal change following no-odor (air) stimulation (left column), but robust change following odor stimulation (right columns). The y-axis depicts instantaneous power at each frequency bin (logarithmically spaced) between 1–100 Hz, *Z*-scored relative to the 1s preceding sniff onset at each frequency bin across all trials. Dotted line marks sniff onset, and grey line indicates average respiratory waveform per condition. Odor conditions are sorted from greatest to least power separately for each subject. (**B**) Odor vs. no-odor difference plots (*Z*-normalized to shuffled null distribution) show significant time-frequency clusters (black outlined areas) in each subject, generally centered at theta frequency and within the first 500 ms post-sniff (cluster corrected at $p < 0.05$). See also Figure S3 and S4.

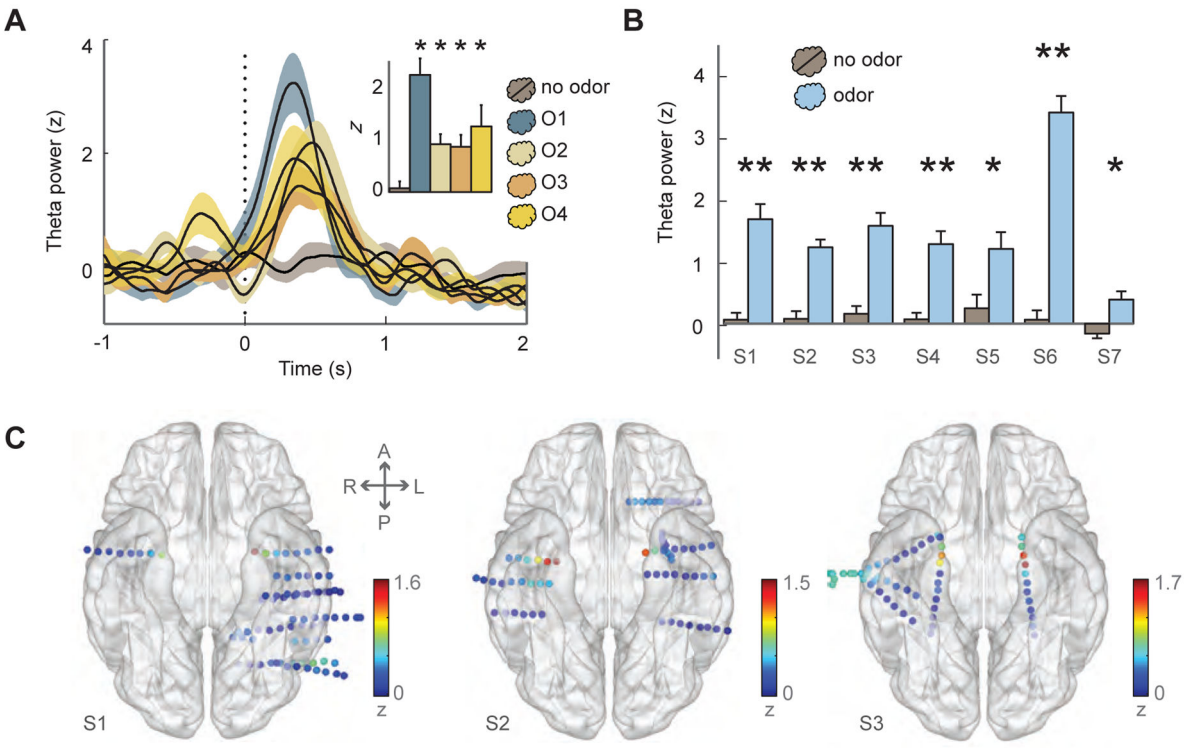


**Figure 3.**

Odor-elicited piriform theta power is robustly observed across stimuli and subjects. (**A**) Example time-course data from one subject (S1) show an increase in trial-averaged theta power for each odor condition in PPC, time-locked to sniff onset (vertical dotted line), without noticeable change for the no-odor condition (means ± S.E.M.). *Inset*, average theta power between 0–500 ms after sniff onset for each condition, compared to no-odor condition, corrected for multiple comparisons (odor 1: $t_{19} = 5.5$, $p = 0.001$; odor 2: $t_{22} = 3.5$, $p = 0.001$; odor 3: $t_{23} = 3.0$, $p = 0.003$; odor 4: $t_{18} = 2.6$, $p = 0.007$). (**B**) For each subject, the average theta power between 0–500 ms after onset was significantly higher in PPC/amygdala for odor conditions (pooled across odors) than for the odorless air condition (**, $p < 0.05$ after multiple comparisons correction; *, $p < 0.05$ before Bonferroni correction). (**C**) Electrode-specific spectral power in the theta band (averaged between 0–500 ms post-onset for the odor condition) for subjects S1–S3 is mapped to the corresponding electrode position on the ventral view of a transparent 3-D brain image, highlighting the prominence of odor-induced theta (yellow-to-red colors) at the anterior medial temporal lobe in the vicinity of PPC. Dots on brain, electrode contacts. Color scale, *Z*-normalized power. A, anterior; L, left; P, posterior; R, right. See also Figure S5.

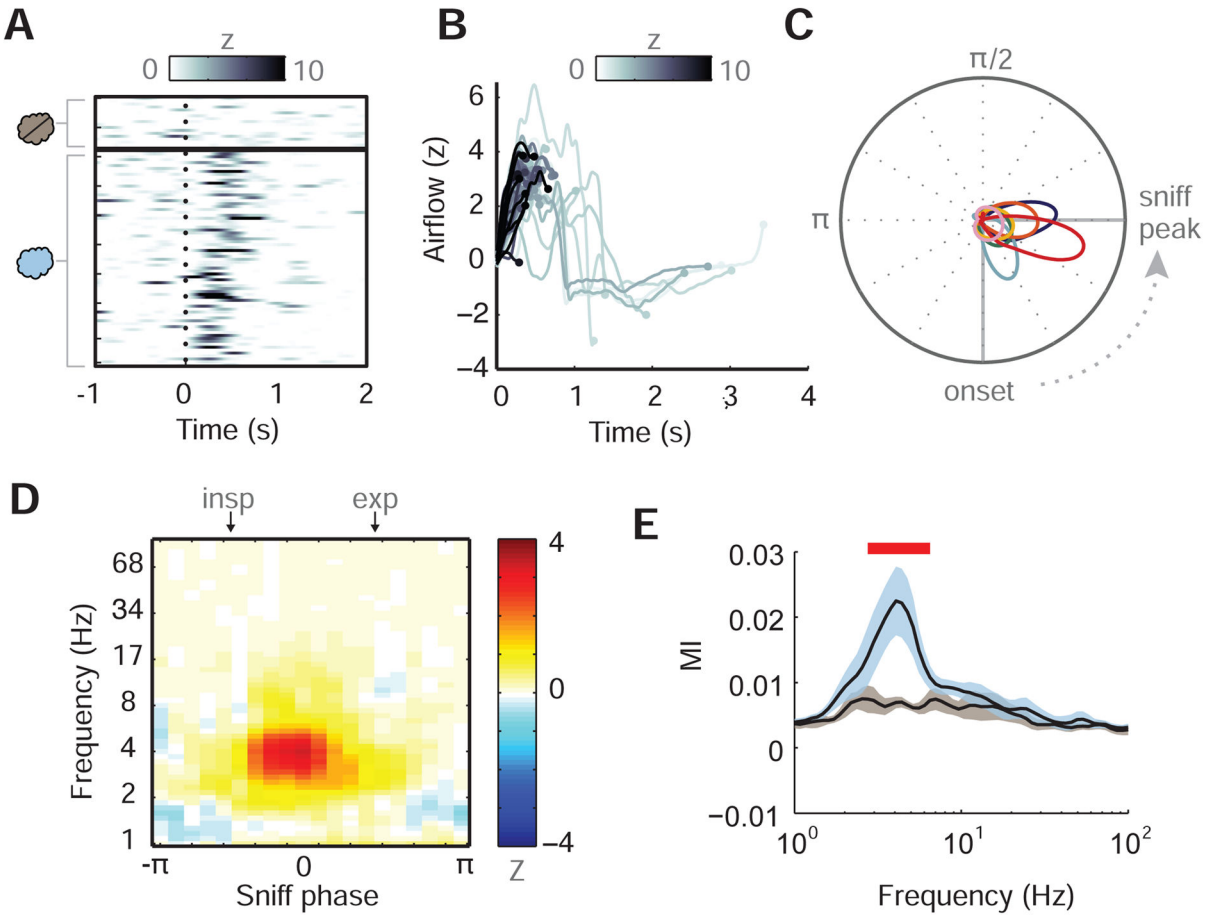


**Figure 4.**

Piriform theta power is locked to respiratory phase across individual trials. (**A**) Single-trial time-course plots of piriform theta power (*Z*-normalized, relative to baseline) in subject S1 reveal consistent effects for odor conditions across trials (rows). Trials sorted first by no-odor condition (n=18 trials), then by odor condition (n=74 trials) in chronological order. (**B**) Trial-specific respiratory waveforms (from subject S1) during odor stimulation, time-locked to inspiratory onset at t = 0 s, in which each waveform is shaded according to the maximal *Z*-scored theta power in PPC. Each respiratory trace is terminated at the time point when piriform theta power was maximal, and shows that trials with higher theta power (dark grey) occurred earlier during inspiration. (**C**) Subject-specific graphs of the probability density functions of the sniff phases at which maximal theta occurred across each odor trial in PPC are plotted along the unit circle. Each color indicates a different subject (see Figure 1A for legend). Circular means of the subject-specific respiratory phase distributions are plotted along the circumference and show clustering of odor-induced piriform theta power between the onset and peak of the sniff. (**D**) Illustrative mean differences across subjects for PPC amplitude at each sniff phase bin (between –π and π) and amplitude frequency bin (between 1 and 100 Hz). Beginning of inspiratory and expiratory phases are marked at top of plot. (**E**) Mean modulation index (MI) across subjects at different frequency bins for both odor (blue) and no odor (grey) conditions. Error bars represent S.E.M. of resampling distribution per

condition, and red line denotes frequency bins where odor MI was significantly greater than no odor MI.

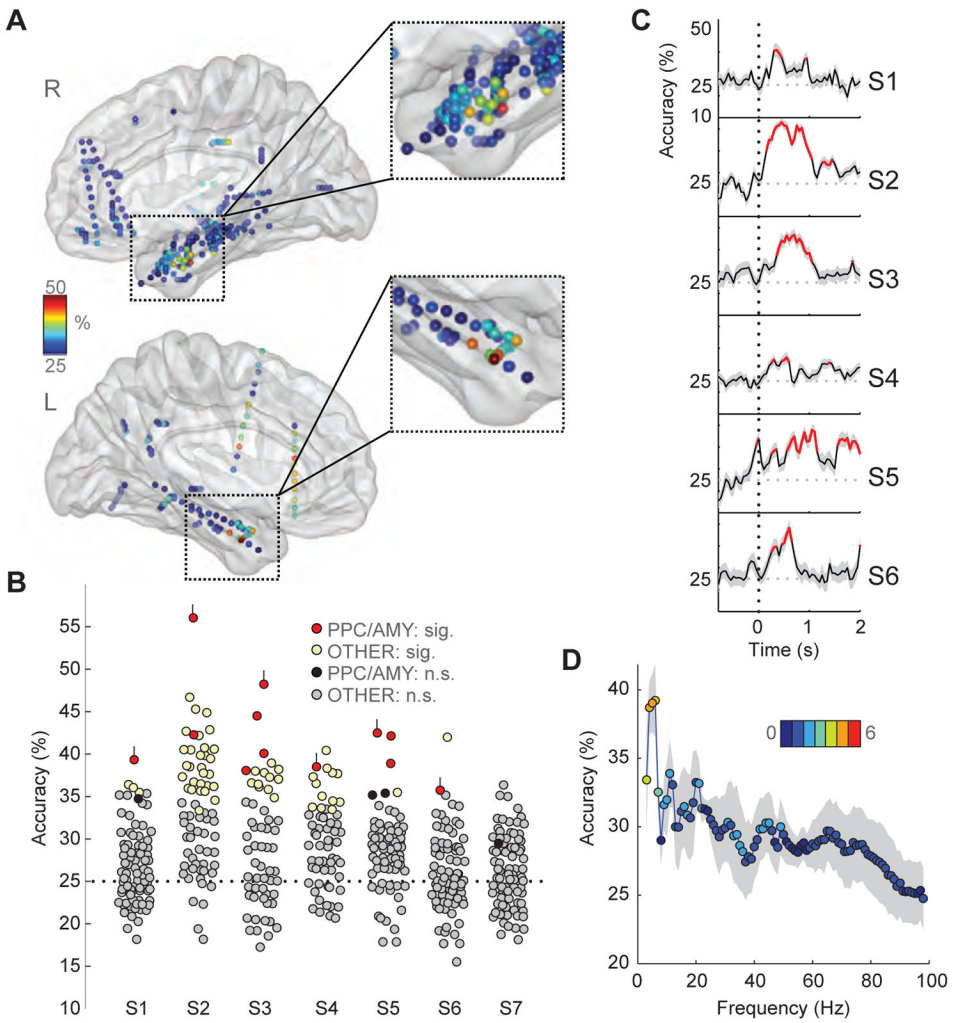


**Figure 5.**

Odor information decoding from oscillatory activity in PPC. (**A**) Classification accuracy of odor decoding from broadband (1–100 Hz) activity from each electrode and each subject was mapped onto the corresponding position on sagittal views of a 3-D transparent brain in MNI space. Data from all subjects are depicted here and show that discrimination of the four odors was consistently high in the anterior medial temporal lobe (orange to red colors). Color bar, accuracy level; chance, 25%. (**B**) Four-way odor classification accuracies across electrodes are plotted separately for each subject. Electrodes that were significant relative to the null distribution are depicted in red (PPC/AMY) or yellow (non-PPC/AMY). Red-colored electrodes with small vertical lines indicate those selected for further analysis (see **5C–D**). Except for subject S7, classification in the PPC/AMY electrodes was consistently among the highest. (**C**) Subject-specific time-series of multi-class odor decoding for the PPC electrodes identified in **B** reveal that significant classification begins 110 ± 58 ms (mean ± SEM) after sniff onset across subjects. Significant time-points relative to the null distribution are denoted in red. S.D. of resampling distribution are displayed in grey shaded lines. (**D**) Odor decoding accuracy in PPC, conditional on frequency, shows that classification is maximal in the theta-frequency range and is consistently observed in most subjects. Dots:

mean accuracy across six subjects, S1–S6; grey shading: S.D. across subjects; color bar/color of dots: number of subjects (0–6) in which piriform decoding was significantly different relative to a shuffled distribution. Thus for example, the peak data point at 6 Hz indicates that the mean accuracy across six subjects was 39.2%, and that this effect was significant for each of four subjects (pale green dot); the data point at 100 Hz indicates that the mean accuracy across six subjects was 25% (chance), and that this effect was significantly greater than chance in only one subject (medium blue dot).

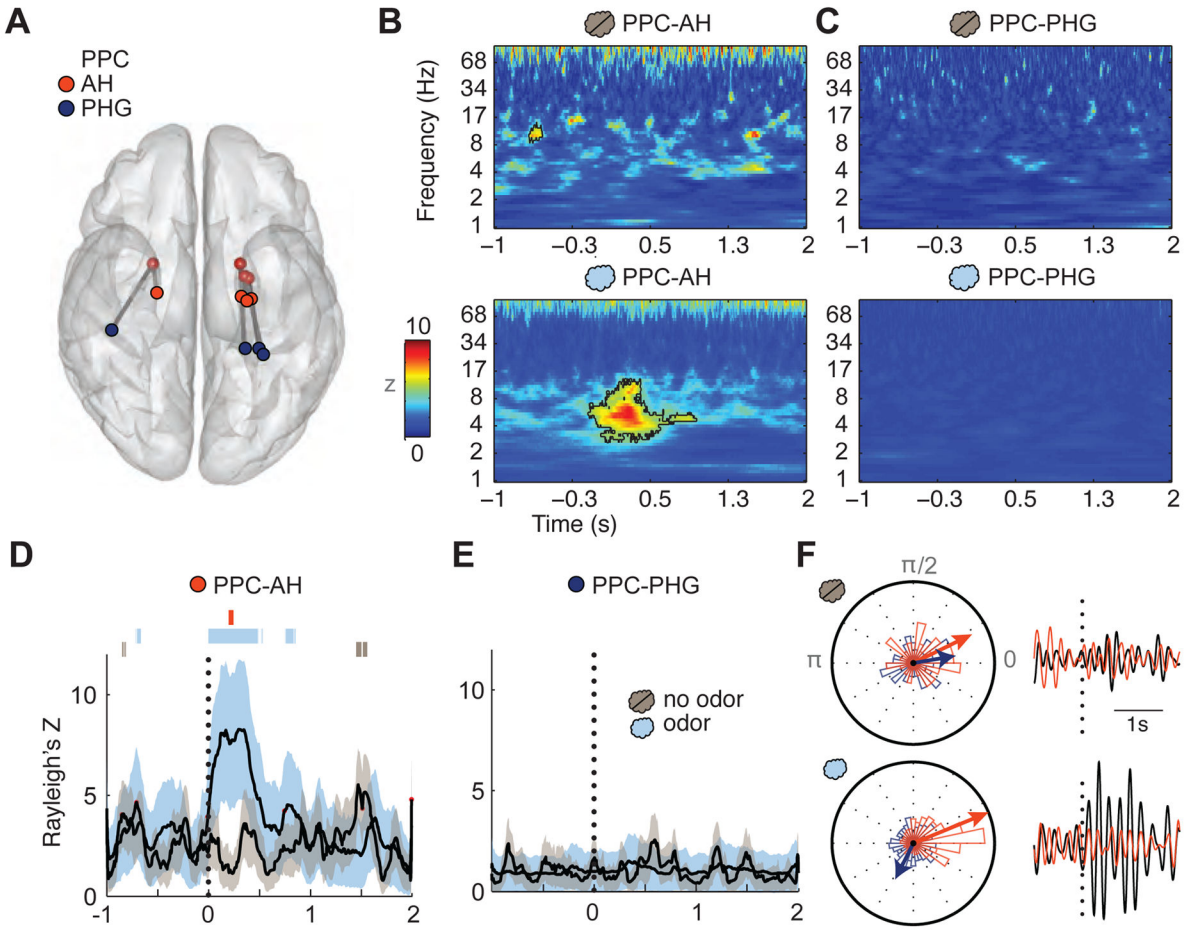


**Figure 6.**

Odor stimulation enhances phase locking between PPC and hippocampus. (**A**) Schematic depiction of the electrode locations in PPC (white), AH (red), and PHG (dark blue) for the four subjects, coregistered and overlaid onto a ventral view of a transparent 3-D brain. (**B**) Time-frequency plots of interregional phase locking between PPC-AH shows minimal change in the PLV following control (no odor) trials (top panel), but a significant change in PLV following odor trials (bottom panel), emerging in the theta-frequency range. Significant time-frequency clusters are outlined with black contours. Data are based on all trials across four subjects. Vertical dotted line, sniff onset at time = 0 s. (**C**) In contrast, interregional phase locking between PPC and PHG showed no evident change in either the no-odor or odor condition. (**D–E**) The PLV time-series, restricted to the theta-frequency range (3–7 Hz), reveals that odor stimulation induces a sniff time-locked increase in coupling between PPC and AH (**D**), but not between PPC and PHG (**E**). Error lines indicate the S.D. of the PLV resampling distribution. Bars above PPC-AH plots in **D**: significant time periods for odor PLV (light blue), no-odor PLV (grey), and odor vs. no-odor PLV (red). (**F**) Circular histograms of the trial-wise phase differences between PPC-AH (red) and PPC-PHG (dark blue) for no-odor (upper left) and odor (lower left) conditions. Vector direction indicates mean phase across trials for each condition and pair, with vector length scaled linearly by circular variance; thus, for conditions in which there is lower variance, or higher consistency,

across trials, the vector length is longer. Right panels: examples of single trial theta-filtered oscillations for PPC and AH (Subject 2, black and red, respectively), aligned to sniff onset, are displayed for no-odor (upper right) and odor (lower right) trials, suggestive of enhanced odor-induced theta coupling between these regions.